

## Huan Liu

Interdepartmental Center for  
Advances in Robotic Surgery (ICAROS),  
University of Naples Federico II,  
80125 Naples, Italy  
e-mail: huan.liu@unina.it

## Bin Zhao

UM-SJTU Joint Institute,  
Shanghai Jiao Tong University,  
800 Dongchuan Road,  
Shanghai 200240, China  
e-mail: zhaobin2014@sjtu.edu.cn

## Zenghui Liu

UM-SJTU Joint Institute,  
Shanghai Jiao Tong University,  
800 Dongchuan Road,  
Shanghai 200240, China  
e-mail: liuzenghui@sjtu.edu.cn

## Kai Xu<sup>1</sup>

State Key Laboratory of Mechanical  
System and Vibration,  
School of Mechanical Engineering,  
Shanghai Jiao Tong University,  
800 Dongchuan Road,  
Shanghai 200240, China  
e-mail: k.xu@sjtu.edu.cn

# Design of a Lightweight Single-Actuator Multi-Grasp Prosthetic Hand With Force Magnification

*Restoring human grasp functions by prosthesis is a long-standing challenge in robotics research. Aiming at prosthetic applications, this paper presents a novel anthropomorphic multi-grasp hand design. The hand is driven by only one motor, and several mechanisms were designed for enhanced functionality. First, a continuum differential mechanism (CDM) was used to generate differential finger motions and to simplify the transmission of the hand. Second, a load adaptive variable transmission (LAVT) was designed to magnify the grasp forces. Moreover, a prismatic clutch is embedded in the hand, to lower the motor's energy consumption. Myoelectric control was implemented using affordable control hardware and sensors. All the above components are integrated in the proposed prosthetic hand, which is an average adult male size and weighs 470 g (including batteries). Experiments, including a preliminary clinical evaluation, were conducted to assess the effectiveness of the hand for prosthetic use. The results show that the hand can perform various grasps and can be a viable option for transradial prosthesis.*  
[DOI: 10.1115/1.4047438]

*Keywords:* compliant mechanisms, grasping and fixturing, prosthetics

## 1 Introduction

Restoring human grasp functionality is a longtime challenge in robotics research. After decades of efforts, several anthropomorphic multifunction prosthetic hands have become commercially available, including the i-Limb Pulse hand (Touch Bionics Ltd.), the Michelangelo hand (Ottobock GmbH.), and the Bebionic V3 hand (Ottobock GmbH.). The mechanical designs, specifications, and performance of those commercial hands can be found in Ref. [1]. Those hands have 2–6 motors for achieving various grasps. However, their current control modes only realize discrete grasp patterns or individual finger control. For instance, seven grasp patterns of the Michelangelo hand [2] and 14 patterns of the i-Limb ultra [3] are preprogrammed. Although the preprogrammed patterns covered major Activities of Daily Living (ADLs), switching between these patterns (e.g., using mobile phone apps) is still inconvenient for amputees.

The human central nervous system (CNS) controls dozens of hand muscles in a coordinated manner. This coordination is referred to as a postural synergy [4]. A fully actuated anthropomorphic robotic hand (e.g., the ones in Refs. [5–7]) can then be controlled to achieve dexterous grasps via two to three channels of biosignals (e.g., electromyography). Although the synergy-based control has been implemented in these research prototypes, this approach might not be practical for prosthesis due to the complexity, affordability, and weight associated with the use of ten or more servomotors. Despite the fact that researchers proposed mechanically implemented synergies using differential pulleys [8], planetary gears [9], linkages [10], and continuum mechanism [11], the complex structures still limit their practical uses.

The adoption of an underactuation mechanism in a robotic hand reduces the number of actuators and the electronics complexity, therefore enhances the hand's reliability and affordability. Furthermore, an underactuation mechanism introduces adaptivity to the hand and alleviates the need of individual finger/joint control, demonstrating a promising way toward affordable hand prosthesis. For the aforementioned reasons, various forms of underactuation mechanisms have been practiced. The utilized mechanisms can be categorized into three types: (i) differential mechanisms, (ii) compliant ones, or (iii) self-locking ones [12]. Each type has application examples in prosthetic hands, including the compliant mechanism in the Toronto/Bloorview MacMillan (TBM) hand [13], the Rehabilitation Institute of Chicago (RIC) arm [14] and the commercial Michelangelo Hand [2], the self-locking mechanism (Geneva drive) in the MANUS hand [15], and the SSSA-MyHand [16]. Differential-based underactuation has even more examples including the linkage-based design [17] and the pulley-based designs [18–21].

Using underactuation mechanisms, robotic hands can realize various grasp patterns under the actuation of a few actuators. Although the advantages of underactuation were demonstrated by the above examples [13–21], underactuated hands are mostly not clinically available (except the Michelangelo Hand by Ottobock). From the technical point of view, compared with dexterous robotic hands, prosthetic hand application imposes multiple additional design challenges, such as anthropomorphism, light weight, grasp pattern versatility, simple control method, etc. These challenges can prevent the translation from the research prototypes [13–21] to commercial prosthetic products.

To address these challenges associated with implementing an underactuated design for prosthetic application, this paper presents the design, optimization, construction, and experimental characterizations of a Multi-Grasp hand with grasp force Magnification (hereinafter referred to as the MGM hand), as shown in Fig. 1.

After weighing the factors such as weight and expense from multiple motors, electronics complexity for sensors, and implementation challenges of multichannel biosignals, the MGM hand adopts

<sup>1</sup>Corresponding author.

Contributed by the Mechanisms and Robotics Committee of ASME for publication in the JOURNAL OF MECHANISMS AND ROBOTICS. Manuscript received October 17, 2019; final manuscript received May 19, 2020; published online July 17, 2020. Assoc. Editor: Ravi Balasubramanian.

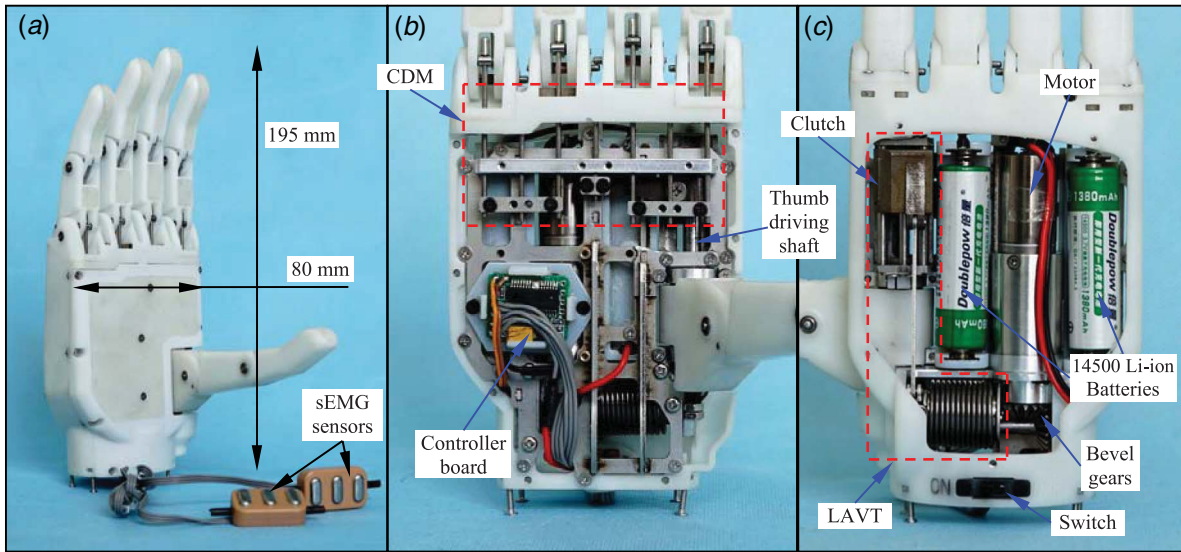


**Fig. 1** The MGM hand: (a) an overview, (b) the palmar side, and (c) the dorsal side

a single-actuator design approach. It possesses: (i) a continuum differential mechanism (CDM) to achieve adaptive grasps, (ii) a load adaptive variable transmission (LAVT) to magnify the gripping force while preserving a high finger closing velocity, (iii) a prismatic clutch to lower the energy consumption of the hand, and (iv) an affordable control hardware with two surface electromyography (sEMG) sensors. The experiments showed that various grasps were formed using the MGM hand. The preliminary clinical evaluation results suggest that the MGM design can be an option for patients with transradial amputation.

This paper is organized as follows. With the overview of the MGM hand summarized in Sec. 2, Sec. 3 details the major components of the hand. Section 4 presents multiple experiments and evaluations with the conclusions and future work summarized in Sec. 5.

## 2 Design Priorities and Overview

The design priorities of hand prostheses have been intensively studied based on questionnaires and analyses [22]. The most important aspects of hand prostheses have been identified as follows:

- (i) Weight is considered a top design priority. Users rate the weight of a prosthetic device as 70 on the scale of 0–100 (not important to most important).
- (ii) Grasp patterns: It is desirable but unrealistic to replicate all the grasps formable by human hands. Luckily, it has been shown that typical ADLs of human hands can be accomplished using a finite set of predefined grasps [23], including power grasp (used in 35% of ADLs), precision grasp (used in 30% of ADLs), and lateral grasp (used in 20% of ADLs).
- (iii) Grasp force and speed: A closing time of 1.01.5 s [13] and a power grasp force of 45 N [24] are considered as adequate for ADLs.
- (iv) Simple control: Despite recent advances in human–machine interfaces, myoelectric control that decodes one or two channels of muscle signals is still the primary solution for practical prosthesis applications, since it is simple to learn to use, noninvasive, and reliable.

Although robotic prosthetic hands are available in the market, their adoption does not prevail [25]. One possible reason for rejecting anthropomorphic prosthetic hands, such as the BeBionic hand and the i-Limb hand, is the heavy weight of the multiple motors introduced by the independently driven finger design [1]. Different design approaches, such as postural synergy [20] and underactuation [26], have been attempted in recent years. However, the

developed prototypes [13–21] are not reportedly commercially available. From the technical point of view, the reason for preventing the translation from the research prototypes to the commercial products may be that these prototypes have not fulfilled all of the four design priorities identified above.

The MGM hand, as shown in Fig. 1, was then developed to fulfill the above design priorities in an anthropomorphic appearance. The total hand length, the palm width, and the wrist thickness of the hand are 195 mm, 80 mm, and 45 mm, respectively. The total weight of the hand is 470 g (including batteries, a controller board, and two sEMG sensors).

The MGM hand has 11 joints, as shown in Fig. 2(a). Each finger has a metacarpophalangeal (MCP) joint and a proximal interphalangeal (PIP) joint, while the thumb has a rotation joint, an abduction (ABD) joint, and an interphalangeal (IP) joint. Among these 11 joints, the thumb's rotation joint is designed to be passive. By manually posing the thumb to different rotational positions, different

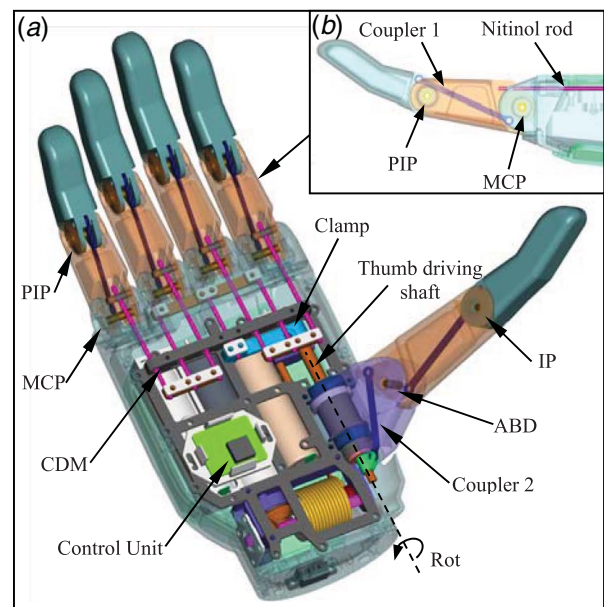


**Fig. 2** Design of the MGM hand: (a) overview of the design and (b) schematic of the index finger

grasp patterns can be realized. Similar designs can be found in the i-limb pulse hand and the Bebionic V3 hand [1].

Since the hand is driven by only one motor, it was decided that the PIP joints shall be coupled to the MCP joints to perform stable grasps. The coupling is realized by a crossed coupler, as shown by the index finger in Fig. 2(b). The thumb shares a similar design, as the IP joint is coupled to the ABD joint. Similar coupled finger designs can be found in Refs. [27–29].

The only motor is placed in the dorsal side of the hand, which drives the LAVT through a pair of bevel gears, as shown in Fig. 1(c). When the fingers are closing, the LAVT works as an ordinary slider-crank mechanism and provides higher digit-closing speed before the fingers encounter an object. Once the fingers are contacted with the object, the output force of the LAVT is magnified as two spring-loaded links start to fold to each other and result in a shorter crank.

To realize adaptive grasps as well as simplify the hand actuation, the CDM is used to drive the fingers, as shown in Figs. 1(b) and 2(a). The CDM has one driving backbone and four driven backbones for four differential outputs. The driving backbone of the CDM is coupled to the driving shaft of the thumb flexion/extension, while the four differential outputs of the CDM are connected to the rest four fingers. Therefore, once the motor is energized, all the digits move simultaneously. As shown in Fig. 1(b), the shaft, which drives the thumb's flexion/extension, is aligned with the thumb's rotation joint axis and supported by the linear bearings. Therefore, the flexion/extension is not influenced as the thumb is manually rotated to different positions for different grasp patterns.

A prismatic clutch is arranged in the transmission, as indicated in Fig. 1(c). The clutch can be locked and unlocked by the slider of the LAVT. Once an object is grasped by the hand, the power supply to the motor can be switched off since the clutch will hold the position and the grasp force is maintained. This feature alleviates the need for a larger battery, which contributes a lot to reducing the weight of a prosthetic hand.

A controller board and two sEMG sensors from Danyang Artificial Limb Co., Ltd., China were adopted to realize myoelectric control. Usually the batteries of transradial prostheses are placed in the forearm socket. In the presented design, two batteries are able to be embedded in the palm to realize a more self-contained design, as shown in Fig. 1(c). This design feature can offer a better solution for amputees with distal transradial amputation or even wrist disarticulations since no extra space in the socket will be required to house the batteries.

### 3 Design Descriptions and Analyses

This section elaborates the designs and analyses of the major components of the hand. Section 3.1 describes the CDM which generates differential finger movements. Design and optimization of the LAVT is presented in Sec. 3.2. Section 3.3 reports the prismatic clutch design and Sec. 3.4 details the myoelectric control realization.

**3.1 Continuum Differential Mechanism.** Various differential mechanisms can be found in a wide spectrum of mechanical systems, since the presence of such device introduces a level of adaptivity. Birglen and Gosselin classified the commonly used differential mechanisms in robotic hands into four different forms: (i) the pulley-based, (ii) the linkage-based, (iii) the gear-based, and (iv) the fluidic T-pipe-based [30]. A recent categorization proposes the kinematic differential mechanisms (KDMs) and the CDMs [31]. The KDMs generate differential outputs from the motions of the kinematic pairs, while the CDMs generate differential outputs via redistributions and/or deformations of their own materials and structures.

The working principle of the utilized multi-backbone CDM is explained as in Fig. 3(a). The CDM consists of a base link, an end link, and an input and two output backbones. All the backbones

are made from super-elastic nitinol rods. The backbones are attached to the end link and can slide in the holes in the base link. A force (indicated by the middle arrow) acts on the input backbone to generate two outputs (indicated by the arrows on both sides) to push external objects. If the load on the left is bigger, continuing to pull the input backbone will bend all the backbones to the right due to the elasticity of the backbones. As shown in Fig. 3(a), the left backbone is stopped but the right one will be continuously driven. Thus, two differential outputs are generated. Once the input force is removed, the CDM will restore the straight configuration because of the intrinsic elasticity of the mechanism. The CDM can provide both pushing and pulling outputs since the backbones can be pushed or pulled. Detailed modeling and analysis of the CDM can be found in Ref. [31], where the bent backbones are modeled as circular arcs.

The CDM generates differential outputs from its elastic deformations, rather than the motion of kinetic pairs of conventional differential mechanism (e.g., pulley-based and linkage-based mechanisms). Due to the backbones' intrinsic elasticity, the CDM does not require any tension-keeping component, which is essential for tendon-based differential mechanisms. Thus, the CDM is advantageous in terms of light weight, structural simplicity, and compactness.

Since only one motor is used to drive all five digits, a two-stage CDM is designed, as shown in Fig. 3(b). The Stage-1 CDM generates two outputs, and the outputs act as the inputs of the two Stage-2 CDMs. Therefore, four differential outputs are produced for the four fingers, while the thumb is directly driven through the thumb driving shaft. The driving backbone of the CDM and the thumb driving shaft are rigidly coupled, as indicated in Fig. 2. Hence, all the five digits close and open simultaneously. When the hand is grasping an object with the thumb opposites other four fingers,

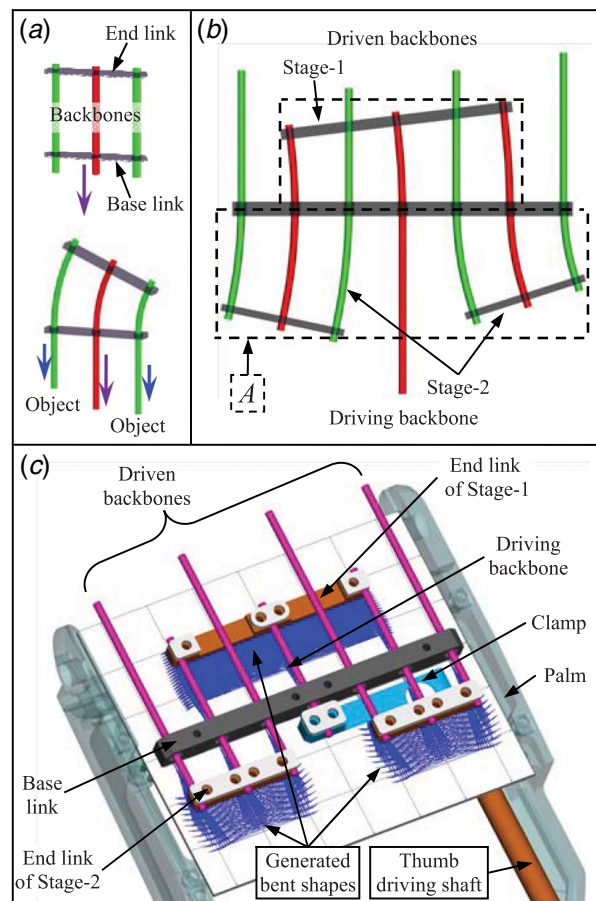


Fig. 3 The CDM: (a) a general planar form, (b) a two-stage planar form, and (c) the two-stage implementation in the palm

the four fingers will adapt to the shape of the grasped object due to the two-stage CDM. During the grasping process, if one of the four fingers encountered the object first, the corresponding backbone is stop. However, other backbones are still able to pull to further close the other fingers, until all the fingers contact the object. Thus, an adaptive grasp is formed by the hand. Grasping of different objects shapes results in different pulling distances on the four output backbones. For a given grasp, a specific bent shape of the two-stage CDM will be formed, as exemplified in Fig. 3(b).

In the presented design, all the backbones are made from  $\Phi 1.5$  mm nitinol rods. The distances between the four output backbones are 20 mm. They are determined according to the finger separation and palm width of the hand. Then, the width of the Stage-1 and Stage-2 CDM can all be determined by evenly distributing the backbones.

To assure that the CDMs can be housed in the palm and will not interfere with other structures, the lengths of the CDMs are optimized toward a minimal area  $A$ , as shown in Fig. 3(b). The area  $A$  comprises two rectangles, which contains the area swept by the Stage-1 CDM and the area swept by the two Stage-2 CDMs, respectively, referring to Fig. 3(b).

Although the shorter the CDM the smaller the area  $A$ , a short CDM may result in large bend of the backbones, which violate the strain limit of the nitinol rod (usually between 4% and 6%). Therefore, the lengths of the two stages of CDM were optimized toward the smallest  $A$ , given the constraints that under every possible CDM bent configurations (as if the hand is grasping various objects), the strains should be always smaller than 3%.

The optimization was implemented by exhaustive enumeration of the design variables (the lengths of the two stages) as follows. First, the length of the Stage-1 CDM was enumerated from 12 mm to 50 mm, while the length of the Stage-2 was between 1 mm and 50 mm. In the enumeration, the lengths were discretized in increments of 1 mm. Then, given a candidate design (i.e., a combination of lengths of the two stages), the strain of the backbones, in any cases of the hand configurations, was checked to see whether the strain always remain under 3%. The hand configurations are exhaustively traversed by enumerating all the possible combinations of actuation of the four fingers. The actuation of each finger is between 0 mm and 12 mm. For the enumeration of the hand configurations, the actuations were also discretized with increments of 1 mm. If the constraint on the strain (<3%) is satisfied by a given combination of the CDM lengths, the area  $A$  that is swept by the CDM is calculated. Finally, the length combination that gives the smallest  $A$  was determined as the optimal design of the CDM lengths.

While enumerating the possible CDM configurations, one assumption was made as follows. Since each output backbone is pulled for about 12 mm to fully close a finger, it is assumed that the difference in the pulling lengths between adjacent output backbones shall be less than or equal to 6 mm (half of the total actuation). Without this constraint, the CDM would be considerably longer and the palm would be unnecessarily big, simply to include the hand poses that do not often occur in ADLs.

By the above optimization, the length of the Stage-1 CDM is determined as 18 mm, while that of the Stage-2 is 8 mm, as all the digits are fully extended. The lengths of the Stage-2 CDM are short because the Stage-2 CDM will be lengthened while pulling to close the fingers. The generated bent shapes were overlaid back to the palm as shown in Fig. 3(c) to make sure the CDM will not interfere with the palm and other structures in any cases of grasps.

The CDM of the MGM hand enables multiple grasp patterns by the actuation of a single motor. Compared with some commercial hands with five or six motors, for example, the BeBionic V3 Hand and the i-Limb hands, the weight of the MGM hand is reduced by using the CDM and one motor. In addition, the CDM of the MGM hand measures only 17 g.

**3.2 Load Adaptive Variable Transmission.** The grasping process of either a robotic hand or a human hand can be roughly

divided into two phases: (i) the approaching phase, in which the fingers of the hand are approaching the object with relatively high speed; (ii) the tightening phase, in which the digits gradually exert forces on the object. It is desirable that a prosthetic hand can operate at high speed in the approaching phase and can also generate large force to ensure powerful grasp in the tightening phase. However, the output force of a mechanism with a constant transmission ratio is inversely proportional to the output speed, if the power of the actuator is kept constant. Thus, a constant ratio cannot meet the conflicting demands of generating both high-speed and large force output. Motor with higher power rating can be used to increase the force output, but additional weight of the motor will be introduced. Particularly, weight is considered as a top design priority of prosthetic hands [22].

Several robotic hands with variable transmissions were designed to meet the needs of the two ends. Usually these transmissions were designed to be passively variable, in order to simplify the designs of the hands. The variation can be either discrete or continuous. Discretely variable transmission switches between few (usually two) ratios. For example, the transmission of a three-fingered gripper [32] switches between a higher state (by spur gears) and a lower one (by a sprag clutch), according to the load on the digits. On the other hand, the continuously variable transmission (CVT) offers continuous transmission ratio changes. Takaki and Omata proposed two finger designs with CVTs based on spring-biased five-bar linkages [33] and eccentric pulleys [34]. Elastomeric pulley with passively variable radius can also offer continuous variable transmission ratio for prosthetic hand [35].

Considering that a robotic hand demands basically a lower reduction ratio for high speed in the approaching phase and a higher deduction ratio for large force in the tightening phase, a variable transmission switching between the two ratios is suitable for our application. Thus, to magnify the grasp force of the MGM hand while preserving its digit speed, the LAVT was designed and optimized. As shown in Figs. 4(a)–4(c), the LAVT is essentially a slider-crank mechanism, but the crank was replaced by two serially connected links (link-1 and link-2) and preloaded by a torsional spring with stiffness  $k_s$ . As an input torque  $\tau_{in}$  exerts on the link-1, a force  $\mathbf{f}_3$  is produced on the link-3, then the slider-2 with a load  $\mathbf{f}_{load}$  is driven. The right-handed angle  $\theta_a$  from link-1 to link-2 is limited in  $[\theta_{a-min}, \theta_{a-max}]$  by mechanical limits. To ensure high approaching speed, the  $\theta_{a-max}$  is set to  $\pi$  and the total length of the link-1 and link-2 is set to 15 mm, which is set according to the constraint from the anthropomorphic appearance of the hand.

Depending on the magnitude of the load  $\mathbf{f}_{load}$ , the LAVT works in one of the three different modes listed as follows:

- (i) Mode-I: the LAVT works as a normal slider-crank mechanism, as shown in Fig. 4(a). The load is relatively low in the approaching phase, as no external load exerted on the fingers. The load only includes the frictions and the torques of the torsional springs at each digit joints. The torsional spring in the LAVT ensures  $\theta_a = \theta_{a-max}$  and  $\theta_1 = \theta_2$ , as illustrated in Fig. 4(a).

According to the modeling in Fig. 4(a),  $\mathbf{f}_3$  can be obtained by solving the following equations:

$$\begin{cases} l_1 \angle \theta_1 + l_2 \angle \theta_2 + l_3 \angle \theta_3 = [s \quad v_1]^T \\ (l_1 \angle \theta_1 + l_2 \angle \theta_2) \times (-\mathbf{f}_3) + \tau_{in} = 0 \end{cases} \quad (1)$$

where  $\angle \theta = [\cos \theta \quad \sin \theta]^T$ . In this paper, the cross product of two 2-dimensional vectors is defined as  $[a_1 \quad a_2]^T \times [b_1 \quad b_2]^T = a_1 b_2 - a_2 b_1$ .

- (ii) Mode-II: the LAVT works as a spring-biased five-bar linkage, as shown in Fig. 4(b). In the tightening phase, the fingers grasp an object and large grasp force is demanded. If the object is relatively large, the LAVT works as a spring-biased five-bar linkage.

Similarly,  $\mathbf{f}_3$  can be obtained by solving the following equations:

$$\begin{cases} l_1 \angle \theta_1 + l_2 \angle \theta_2 + l_3 \angle \theta_3 = [s \ v_1]^T \\ (l_1 \angle \theta_1 + l_2 \angle \theta_2) \times (-\mathbf{f}_3) + \tau_{in} = 0 \\ (l_2 \angle \theta_2) \times (-\mathbf{f}_3) + \tau_s = 0 \end{cases} \quad (2)$$

where  $\theta_a = \theta_2 - \theta_1 + \pi$  and  $\tau_s = k_s(\pi + \theta_1 - \theta_2)$  is the torque generated by the torsional spring.

- (iii) Mode-III: If the grasped object is relatively small, the LAVT works as a slider-crank mechanism with a shortened crank, since the link-1 and the link-2 folded to each other and they can be considered as a rigid link, as shown in Fig. 4(c).

Then,  $\mathbf{f}_3$  can be obtained by solving the following equations:

$$\begin{cases} l_1 \angle \theta_1 + l_2 \angle \theta_2 + l_3 \angle \theta_3 = [s \ v_1]^T \\ (l_1 \angle \theta_1 + l_2 \angle \theta_2) \times (-\mathbf{f}_3) + \tau_{in} = 0 \end{cases} \quad (3)$$

where  $\theta_2 = \theta_1 + \theta_{a-min} - \pi$ .

As shown in Fig. 4(a), the link-3 pulls the slider-1 with  $\mathbf{f}_3$  via the pin joint at the point-C. Force  $\mathbf{f}_{load}$  on the slider-2, applied by the thumb driving shaft, is the external load the LAVT mechanism

carries. To obtain  $\mathbf{f}_{load}$ , the force transmission from  $\mathbf{f}_3$  to  $\mathbf{f}_{load}$  is modeled as detailed in Fig. 4(d). As shown in Fig. 4(d), the link-3 pulls the slider-1 with  $\mathbf{f}_3$  via the pin joint at the point-C, thus the slider-1 pushes the slider-2 with  $-\mathbf{f}_c$ . Both sliders move on two  $\Phi 3$  mm cylinder guides and subject to the friction with the guides. The statics modeling of the slider-1 and the slider-2 are derived, thus  $\mathbf{f}_{load}$  can be calculated from  $\mathbf{f}_3$  as follows.

The forces on the slider-1 are related as

$$\begin{cases} \mathbf{f}_3 + f_a [\mu \ -1]^T + f_b [\mu \ -1]^T + \mathbf{f}_c = \mathbf{0} \\ [-h_1 \ v_2]^T \times \mathbf{f}_3 + [-h_2 \ 0]^T \times [0 \ f_a]^T = 0 \end{cases} \quad (4)$$

where  $\mu$  is the friction coefficient (a value of 0.2 is used in this investigation),  $f_a [\mu \ -1]^T$  and  $f_b [\mu \ -1]^T$  are the forces exerted by the guide shafts on the slider-1, at the left and the right edges of the slider-1, respectively. The force that slider-2 exerted on slider-1 is denoted as  $\mathbf{f}_c$ . The width measured from the point-C (where  $\mathbf{f}_3$  applied) to the rightmost of the slider-1 is  $h_2$ , while the height measured from the point-C to the guide is  $v_2$ . The width of the slider-1 in contact with the guide is given by  $h_1$ .

For the slider-2,  $-\mathbf{f}_c$  pushes on it as a driving force to drive the load  $\mathbf{f}_{load}$ . The normal force between the guide shaft and the slider-2 is assumed linearly distributed along the axis of the shaft and it is denoted as  $f_e(x)$ . Therefore, the forces on the slider-2 are related as

$$\begin{cases} \int_0^{h_3} \left( \begin{bmatrix} x \\ 0 \end{bmatrix} \times \begin{bmatrix} 0 \\ f_e(x) \end{bmatrix} \right) dx + \begin{bmatrix} 0 \\ v_3 \end{bmatrix} \times \mathbf{f}_{load} = 0 \\ \mu \int_0^{h_3} |f_e(x)| dx + \mathbf{f}_{load} - \mathbf{f}_c = \mathbf{0} \end{cases} \quad (5)$$

where  $h_3$  is the width of the slider-2 and  $v_3$  is the distance between the guide and the thumb driving shaft.

Given a configuration of the LAVT and the input torque  $\tau_{in}$ ,  $\mathbf{f}_3$  can be solved by either Eqs. (1)–(3), depending on the working mode. Then,  $\mathbf{f}_{load}$  can be solved using Eqs. (4) and (5).

The grasp force of the prosthetic hand depends on the  $\mathbf{f}_{load}$  in the tightening phase (mode-II and mode-III). Therefore, an optimization was conducted toward largest force output of the mode-II and mode-III in the entire working range as  $s \in [s_{min}, s_{max}]$ . The objective function is defined as

$$\int_{s_{min}}^{s_{max}} |f_{load}| ds \quad (6)$$

For the LAVT, there are four design variables to be optimized,  $l_1$  ( $l_2$  satisfies  $l_1 + l_2 = 15$  mm),  $l_3$ ,  $\theta_{a-min}$  and  $k_s$ .

Besides the geometric constraints of the linkage, the other important constraint is that the LAVT should work in the mode-I when the digits approach an object. In other words, the torsional spring should be stiff enough to keep the link-1 and the link-2 fully extended when the load is relatively low. Therefore, a hand transmission prototype was built to quantify the actuation force needed in the approaching phase and the force was measured as 11.7 N. In the optimization,  $f_{load}$ , solved by Eqs. (1) and (5), should be larger than 20 N (instead of 11.7 N) for a proper design margin.

The structural parameters of the LAVT, the input torque, and the friction coefficient are listed in Table 1. Simulated annealing algorithm was used to solve this optimization and the optimized design is also listed in Table 1. Using the optimal parameters from Table 1, the LAVT is designed as in Fig. 5, together with the prismatic clutch. The torsional spring is installed on the cylinder-shape link-1, to keep the link-1 and the link-2 extended in the mode-I.

**3.3 Prismatic Clutch.** Locking mechanisms have been widely used in robot designs for maintaining outputs without continued energy consumption. With a locking mechanism, smaller battery with less capacity can be used for a self-contained mechatronic system, such as powered prosthetic hands and legs. In robotic

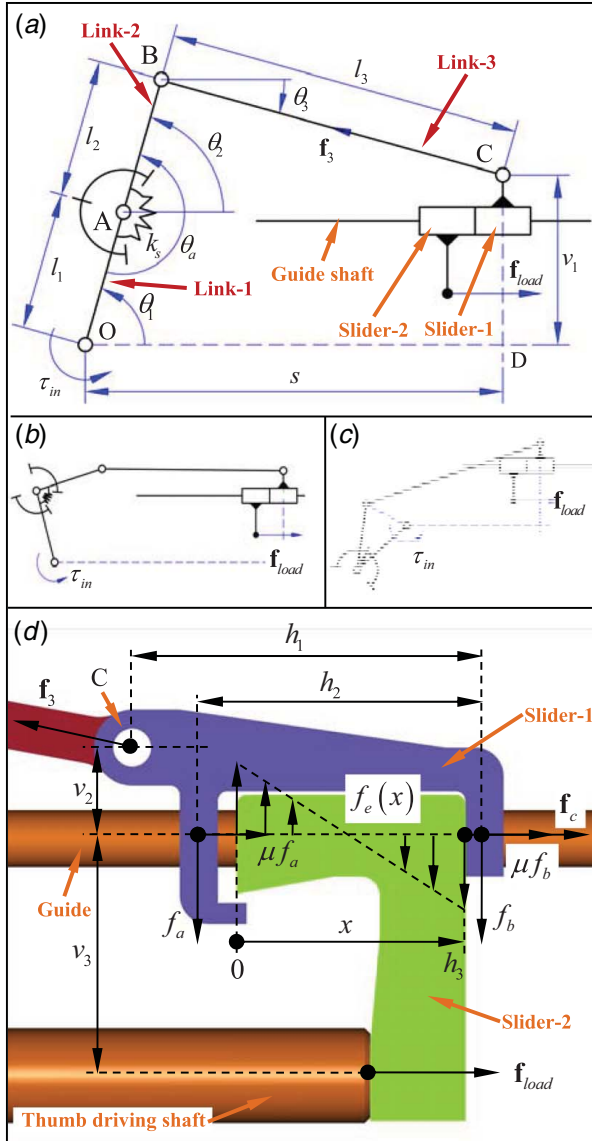
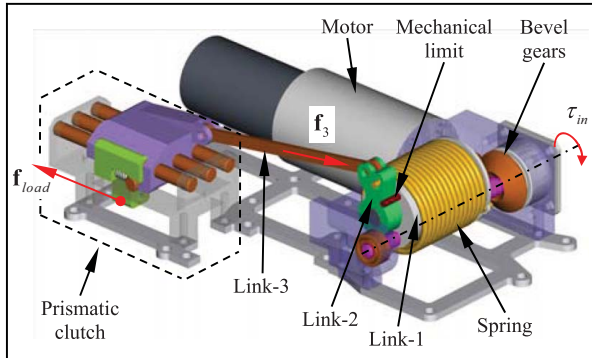


Fig. 4 Schematic and modeling of the LAVT: (a) mode-I, (b) mode-II, (c) mode-III, and (d) the sliders

**Table 1 Parameters of the LAVT**

$h_1 = 18.5 \text{ mm}$	$h_2 = 15 \text{ mm}$
$h_3 = 12 \text{ mm}$	$v_1 = 7 \text{ mm}$
$v_2 = 4.8 \text{ mm}$	$v_3 = 9 \text{ mm}$
$s_{min} = 41 \text{ mm}$	$s_{max} = 54 \text{ mm}$
$\tau_{in} = 1.5 \text{ Nm}$	$\mu = 0.2$
$\theta_{a-max} = \pi$	$\theta_{a-min} = 1/6\pi$
$l_1 = 5.9 \text{ mm}$	$l_2 = 9.1 \text{ mm}$
$l_3 = 46 \text{ mm}$	$k_s = 50.8 \text{ mNm/rad}$



**Fig. 5 Design of the LAVT**

hand designs, the friction-based locking mechanisms were commonly adopted [36]. This type of locking mechanism has various forms, including non-backdrivable transmissions (e.g., worm gears and lead screws), overrunning clutches, and active brakes. Since active brakes need extra actuation and control signals, they may complicate the design of a prosthesis.

After surveying the characteristics of different locking devices, a prismatic clutch was designed for the MGM hand, as shown in Fig. 6. It comprises a base, three parallel guiding shafts, a spring-loaded cylinder, an input, and an output slider (the slider-1 and slider-2 of the LAVT, respectively). With three springs constantly pushing on it, the cylinder is wedged between the angled gap formed by the slider-2 and the base. As the link-3 pulls the slider-1 leftward, the slider-2 moves accordingly. Since the cylinder is wedged between the angled gap, the slider-2 can still hold its position if the driving force is removed. Therefore, if the MGM hand is holding an object, the grasp configuration will be maintained. As the driving link pushes the slider-1 rightward, the

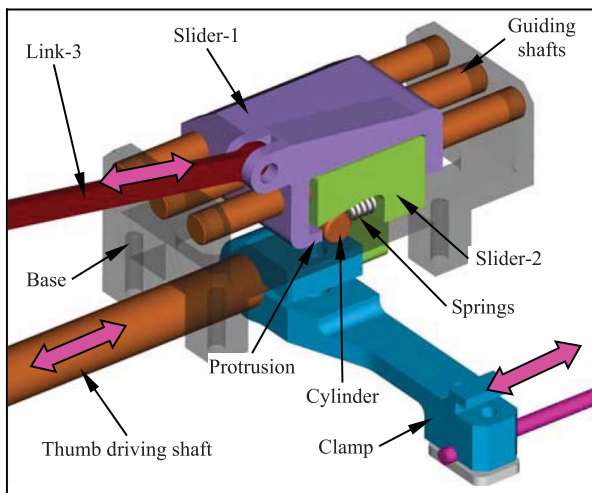


**Fig. 6 Schematic of the prismatic clutch**

protrusion on the slider-1 will push the cylinder out of the wedging position at first, then the slider-2 is unlocked. As the slider-1 pushes further, the slider-2 will be driven accordingly.

The working principle of this clutch resembles the non-backdrivable mechanism of the SmartHand [37], but the proposed design is prismatic and operates in one direction. The presented prismatic clutch possesses several advantages. First, it can lock at any place in the workspace, rather than at limited positions like a ratchet does. Second, it can lock and unlock by the slider-2 of the LAVT, so no extra actuator or control signal is needed. The proposed prismatic clutch is simple. Although it locks in only one direction, this is enough for robotic hand applications, because typically a robotic hand only needs to maintain its gripping force. Additionally, if the digits are accidentally pushed close, the sliders can move leftward freely. This feature allows the digits to flex compliantly, preventing the digits from being damaged.

**3.4 Control and Actuator Hardware.** For the purpose of cost efficiency and reliability, the controller board and the sEMG sensors (see Fig. 1) were brought from Danyang Artificial Limb Co., Ltd, China. They are also used in commercial gripper-like single-DoF prosthetic hands.

A block diagram of the control and actuator hardware of the MGM hand is shown in Fig. 7. The prosthetic hand is powered by two serially connected 14,500 lithium-ion batteries rated at 7.4 V and 1360 mAh. On the controller board, a voltage regulator (78M05, Texas Instruments) is used to produce 5 V direct current (DC) for the microcontroller unit (MCU) STC 89C51 (STC Co.). A H-Bridge motor driver chip (BD6222FP, All ROHM) drives the DC motor (Maxon DCX16S 6 V with a 251:1 gearhead with a power rating of 2.5 W) according to the pulse width modulation (PWM) signal from the MCU. The MCU also detects the current feedback of the motor driver chip. Once the current exceeds the motor stall limit, the power to the motor will be switched off and the clutch maintains the grasp pose.

Two sEMG sensors are powered at 7.4 V DC. To fit the MGM hand to an amputee, the sensors should be embedded inside a customized socket and located separately over the wrist flexor and extensor muscles of the amputee. The sensors detect sEMG signals and generate outputs ranging 0–3.3 V. When the amputee intentionally engages the flexor or the extensor, the voltage output of the corresponding sensor rises. The MCU acquires the amplified sEMG signals and controls the motor in a simple on-off manner. Specifically, once the activation the flexors reached a pre-defined value, the hand is commanded to close. And vice versa, once the extensors are engaged to a certain level, the hand opens. The sEMG thresholds for opening and closing of the hand should be tuned for an individual amputee to assure that the amputee can control the hand with moderate muscle contraction thus muscle fatigue can be avoided.

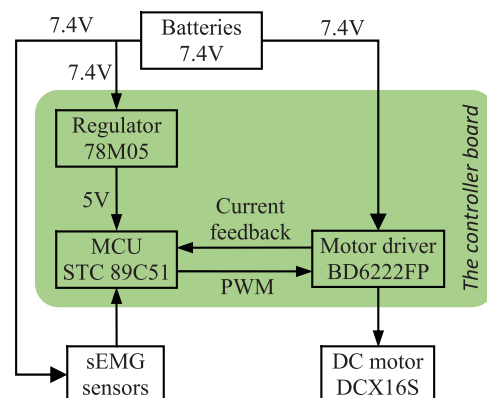


**Fig. 7 Block diagram of the control and actuation hardware**

**Table 2 Specifications of the MGM hand and other prosthetic hands**

	Dimensions (mm)	Total weight (g)	Fully close time (s)	Grasp force (N)	No. of motors	Total motor power (W)	Run time
MGM hand	195 × 80 × 45	470, 408 <sup>a</sup>	0.58	Power grasp: 25.7, pinch: 8.7	1	2.5	3.8 h (2760 grasps)
The hand in Ref. [19]	Unknown	350 <sup>a</sup>	0.9	Power grasp: 5.1, lateral grasp: 4.7	1	4	Unknown
SoftHand Pro-H [21]	Unknown	520 <sup>a</sup>	Unknown	Power grasp: 63, pinch: 20	1	15	4 h (3500 grasps)
RIC hand [14]	Unknown	383 <sup>a</sup>	0.4	Power grasp: 84	2	10	5.4 h
SSSA-MyHand [16]	Unknown	480 <sup>a</sup>	0.37	Thumb: 31.4, digits: 9.4–14.6	3	24	2300 grasps
i-Limb Pulse (medium) [1]	182 × 80 × 45	539	1.2	Power grasp: 136	5	7.5	Unknown
Michelangelo [1]	Unknown	746	0.25	Opposition mode: 70, neutral mode: 15	2	Unknown	Unknown

<sup>a</sup>Weight without battery.

## 4 Experimental Characterizations

The MGM hand was fabricated mostly with 3D printing, while critical transmission and actuation components were made from stainless steel. Its total weight is 470 g, including the batteries, the sEMG sensors and the controller board. The hand can perform about 2760 grasps on one charge of battery. If the grasps are performed at a rate of 5 s/grasp, the hand can support 3.8 h of continuous use. Table 2 presents the major specifications of the MGM hand, together with the hand in Ref. [19], the SoftHand Pro-H [21], the RIC hand [14], the SSSA-MyHand [16], the i-Limb Pulse hand [3], and the Michelangelo hand [1]. The weight of the MGM hand (470 g and 408 g with/without the battery, respectively) is considered lighter than the commercial ones with similar sizes.

The major objective of this section is to experimentally evaluate the capability of the MGM hand and to assess the effectiveness of the hand as a prosthesis. Before testing the MGM hand, the performance of the LAVT, which is an essential component of the hand, was first evaluated.

**4.1 Quantification of the LAVT.** The force magnification properties of the LAVT are quantified using the experimental setup shown in Fig. 8(a). The LAVT and the clutch are installed on a platform according to their relative positions in the hand design. The LAVT and the clutch are shown in Fig. 8(b).

A 3.4 kg weight hung from a  $\Phi 90$  mm pulley was used to generate 1.5 Nm torque, simulating the output of the motor. The slider-2 of the clutch is connected to a force gauge (HP-500 from Yueqing Handpi Instruments Co., Ltd., China with a range of  $\pm 500$  N) by a steel wire. The force gauge is installed on the slider of a linear guide rail. Spacers made of steel plate with 1 mm thickness are inserted between the force gauge and the platform, to place the slider-2 at different positions.

The quantification for each position (i.e., each different  $s$ ) repeated for five times. For comparison, the force outputs of a slider-crank mechanism with a 15 mm crank were quantified as well (also five times for each position). The results are all plotted Fig. 8(c). Using the parameters listed in Table 1, the output forces of the LAVT in the tightening phase were simulated, as shown in Fig. 8(c). The result is composed by two curves which are given by the mode-II and the mode-III separately. For comparison, the force outputs of an ordinary slider-crank mechanism with a 15 mm crank were also simulated and are shown in Fig. 8(c).

The experiments show that the average force output of the slider-crank mechanism in the whole workspace is 58.4 N, while the LAVT generates an average force output of 146.7 N, which is 2.5 times larger. Compared with the theoretical values that are calculated with a friction coefficient of 0.2, the results of both

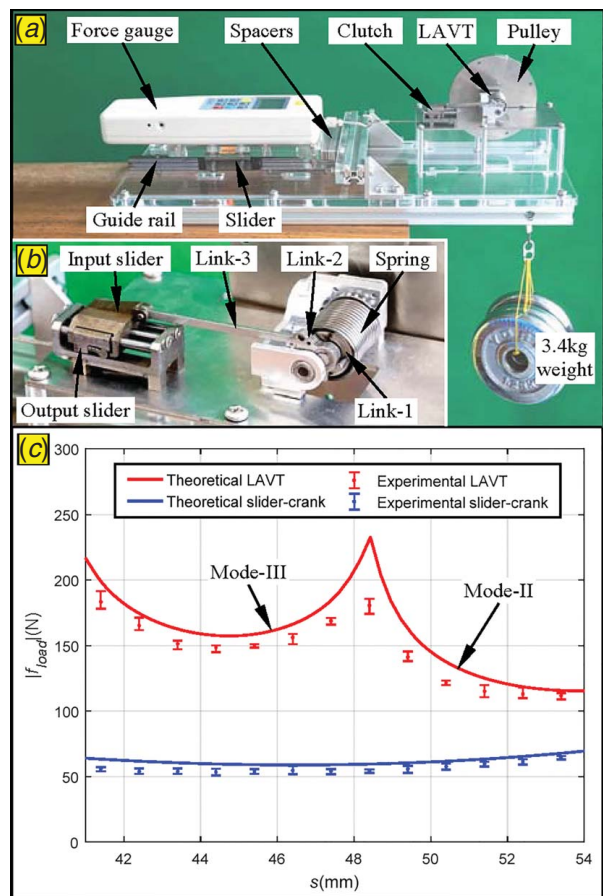


**Fig. 8 Quantification of the LAVT: (a) experimental setup, (b) details of the LAVT and the clutch, and (c) comparison between the results and the theoretical values**

mechanisms are slightly smaller, probably due to the additional friction in the linkage under the loads.

**4.2 Grasping Capabilities.** It is paramount that the MGM hand can perform various grasps so a set of grasping experiments were conducted to check the hand's capabilities.

The experimental setup is shown in Fig. 9(a). The batteries and the control hardware of the hand were not used in this set of experiments. The hand's motor is powered by a linear DC power supply. The power supply has an adjustable built-in current limit switch so

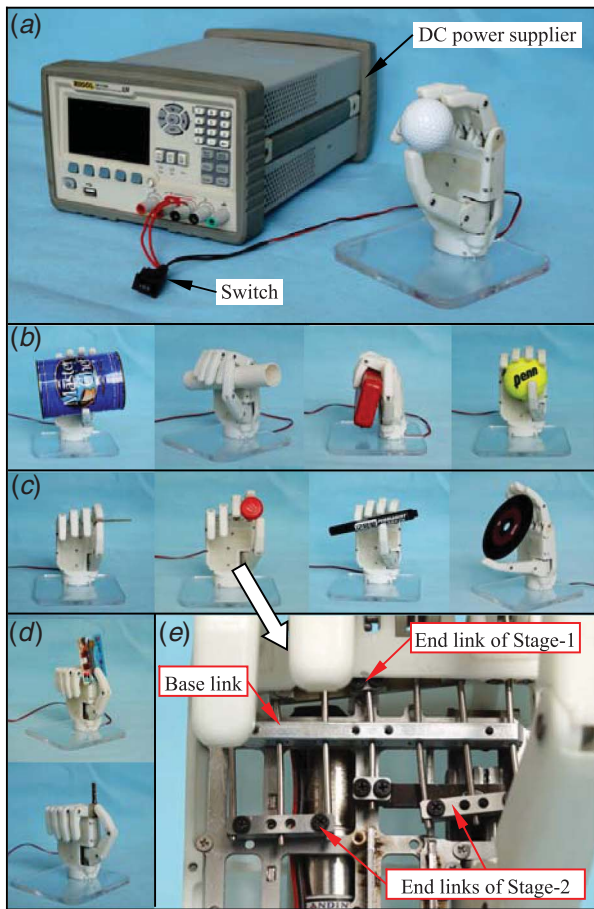


**Fig. 9 Grasp pattern demonstration: (a) experimental setup, (b) power grasps, (c) precision grasps, (d) lateral grasps, and (e) CDM bent shape example**

that the motor can be protected during grasps. A double pole double throw switch was used to turn on/off the motor. Direction of the current can be changed to rotate or reverse the motor so as to open and close the hand. Then, the hand was used to grasp various daily objects, as shown in Figs. 9(b)–9(d). Some of the objects are from the YCB object set [38].

The motor is always powered on at 7.4 V with the current limit is set to 1.5 A (the stall current of the motor), until the grasp is completed and the motor is stalled. Then the power is turned off. The grasp configurations were maintained by the prismatic clutch inside the hand.

The hand can realize three typical grasp patterns: power, precision, and lateral grasps. For the power grasps in Fig. 9(b) and the precision grasps in Fig. 9(c), the thumb was manually posed to the opposite position. The hand adapted to the shapes of the objects, due to the differential outputs generated by the CDM. For the lateral grasp, the thumb was manually adjusted to the lateral position. A card and a key were grasped by the thumb and the lateral of the palm, as shown in Fig. 9(d).

The bent shape of the CDM, as the hand pinching a bottle cap using three digits, is shown in Fig. 9(e). The output backbones driving the index and middle finger were stopped by the loads, the backbones driving the ring and the little finger continued to pull and the CDM bent to the shown shape.

**4.3 Quantification of the Grasping Forces.** Before quantifying the grasp forces, the digit speed was experimentally measured through analyzing videos of the hand performing open/close motions in free space. During the movements, the hand was

powered at 7.4 V for the entire duration of motion. Results showed that fully closing the hand took 0.58 s, which is faster than the 0.8 s of the i-Limb Pulse hand and 1.0 s of the Bebionic V3 hand [1].

The quantifications of the grasp force were performed as shown in Figs. 10(a)–10(c). For the power grasp and five-finger pinch, an ATI Nano 17 force/torque sensor was installed inside a  $\Phi 60$  mm 3D-printed cylinder. For the tripod pinch, the sensor was installed inside a  $\Phi 40$  mm ball (golf ball size). In order to quantify the forces of different grasp patterns, the sensor was grasped in different configurations (power grasp, five-finger pinch, and tripod pinch), as shown in Figs. 10(a)–10(c). The results are plotted in Fig. 10(d) when the motor is powered at 7.4 V and the limiting current increases from 0.3 A to 1.5 A. Each grasp configuration was repeated for five times. The average grasp forces of the power grasp, five-finger pinch, and tripod pinch at 1.5 A current are 25.7 N, 8.7 N, and 6.0 N, respectively. The power grasp force is lower than the threshold of 45 N [24] and lower than some of the hands listed in Table 2. However, it is worth noting that the MGM hand uses only one motor and the power rating of the motor is the only 2.5 W, which is the lowest among the hands. By adopting a gear box with doubled reduction ratio (502:1), the power grasp force can be approximately doubled (from 25.7 N to 51.4 N). The closing time will be increased from 0.58 s to 1.16 s, but it is still acceptable according to Ref. [13]. The grasp force of the hand can be further increased by adopting a motor with higher power rating, for example, the Maxon DCX16S with graphite brushes which has the same size as the one of the MGM hand but a power rating at 4.5 W.

**4.4 Preliminary Clinical Evaluation.** Preliminary clinical evaluation was conducted to examine the effectiveness of the MGM hand for prosthetic application, using the integrated control hardware. As shown in Fig. 11(a), the hand is mounted on a customized socket via a passive wrist. The pronation/supination of the wrist can be manually configured to different positions. The

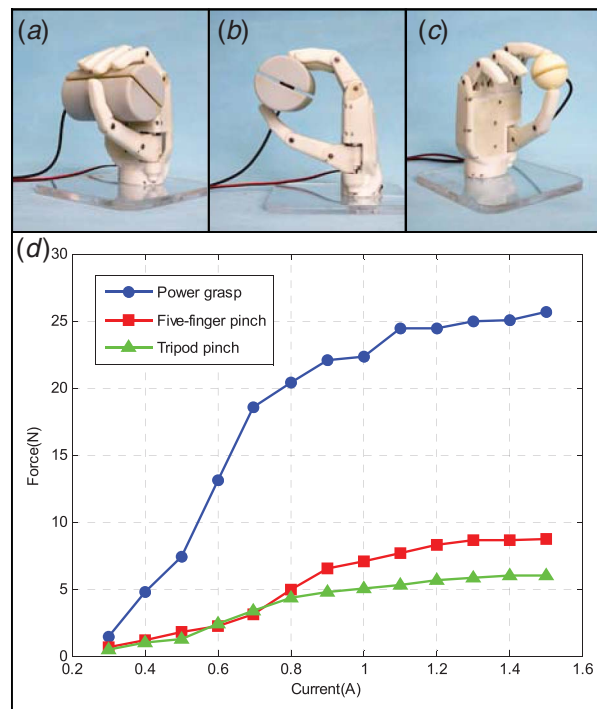


**Fig. 10 Grasp force quantifications: experimental setup of (a) power grasp, (b) five-finger pinch, (c) tripod pinch, and (d) measurement results**

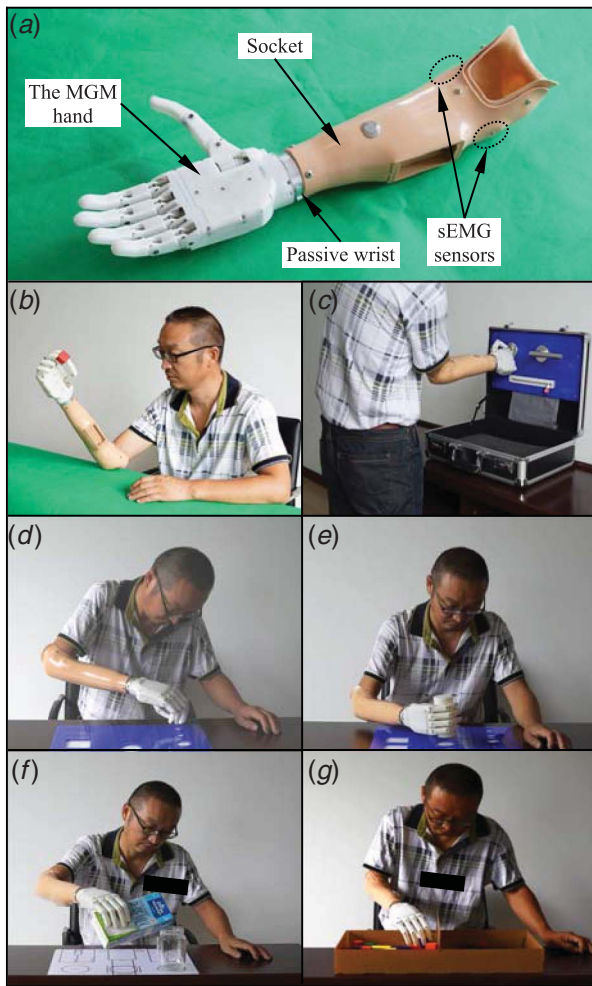


**Fig. 11 Preliminary clinical validations: (a) a transradial prosthesis assembly, (b) an amputee wears the MGM hand, (c–f) the amputee performs some ADLs, and (g) the amputee performs the BBT**

sEMG sensors are installed inside the socket. The prosthesis was then fitted to a transradial amputee, as shown in Fig. 11(b).

After being exposed to the prosthesis for a few minutes, the subject could easily perform different grasp patterns and completed the evaluation. The amputee was invited to perform some ADLs using the MGM hand, such as turning a key, picking up a small object from a surface, holding a cylinder, and pouring milk from a carton, as shown in Figs. 11(c)–11(f), respectively. The subject did not report any difficulty on controlling the hand. His quick adaptation is partially due to the experience of using a commercial single-DoF prosthesis with the same on–off control method.

To quantify the functionality of hand prostheses, several measures have been established [39]. Due to the availability of the testing kit, the Box and Blocks Test (BBT) [40] was followed in this study. The BBT, as shown in Fig. 11(g), is designed to assess unilateral gross manual dexterity. Participant was seated at a table, facing a rectangular box that is divided into two square section of equal dimension by a partition. One hundred and fifty 25 mm colored wooden blocks were placed in one section. The subject was instructed to move as many blocks as possible, one at a time, from one section to the other for a period of time (2 min in this research). The BBT is scored by counting the number of blocks carried over the partition during the trial period. The participant scored 21.7 in average in three consecutive trials (31, 19, and 15 blocks, respectively). The number showed a decrease, probably because the forearm muscles fatigued in the following two trials.

It is hard to find a BBT score of an amputee using a transradial prosthesis for comparison. To give a rough reference, the subjects who used transhumeral prostheses scored 11–20 points [14,41].

Although further studies involving more participants are demanded to comprehensively validate the hand, this preliminary result suggests that the hand successfully met the basic requirements of prosthetic applications.

## 5 Conclusion and Future Work

This paper reports the design, optimization, construction, and preliminary clinical evaluation of the MGM hand, a lightweight single-actuator multi-grasp prosthetic hand with force magnification. This development aims at providing one viable prosthesis option for transradial hand amputees.

Three main features have been integrated into the MGM hand: (i) a CDM for adaptive grasps, (ii) a LAVT to magnify grasp forces, and (iii) a prismatic clutch to maintain the grasp poses. It has been demonstrated that various grasps can be formed by this single-actuator hand, indicating the effectiveness of this design. An amputee can easily control the hand via two sEMG sensors. Preliminary clinical results suggest that the hand successfully met the requirements of prosthetic applications.

A few improvements are expected to be included in the near future. First, a cosmetic glove is needed and the structure of the digits and palm should be modified accordingly, to adapt the glove. As indicated by the comparison with other hands, the grasp forces of the MGM hand are lower than commercial hands, due to lower power rating of the motor. The grasp force can be increased by adopting a gear box with higher reduction ratio or a motor with higher power rating. The two measures can be also implemented in combination to further increase the grasp force.

## Funding Data

This work was supported in part by the National Natural Science Foundation of China (Grant No. 51722507) and in part by the National Program on Key Basic Research Projects (Grant No. 2011CB013300).

## Conflict of Interest

There are no conflicts of interest.

## References

- [1] Belter, J. T., Segil, J. L., Dollar, A. M., and Weir, R. F., 2013, "Mechanical Design and Performance Specifications of Anthropomorphic Prosthetic Hands: A Review," *J. Rehabil. Res. Dev.*, **50**(5), pp. 599–618.
- [2] Ottobock SE & Co. KGaA, "The Michelangelo® Hand in Practice: Therapy and Rehabilitation," Brochure, <https://www.ottobock.com/media/local-media/prosthetics/upper-limb/michelangelo/files/michelangelo-therapy-brochure.pdf>, Accessed June 15, 2020.
- [3] Touch Bionics Ltd., "i-Limb Hand User Manual," User manual, [https://www.touchbionics.com/sites/default/files/files/MA01382\\_i-limb%20hand%20user%20manual\\_TBby%C3%96ssur\\_Q1.pdf](https://www.touchbionics.com/sites/default/files/files/MA01382_i-limb%20hand%20user%20manual_TBby%C3%96ssur_Q1.pdf), Accessed June 15, 2020.
- [4] Santello, M., Flanders, M., and Soechting, J. F., 1998, "Postural Hand Synergies for Tool Use," *J. Neurosci.*, **18**(23), pp. 10105–10115.
- [5] Wimböck, T., Jahn, B., and Hirzinger, G., 2011, "Synergy Level Impedance Control for Multifingered Hands," Proceedings of 2011 IEEE/RSJ International Conference on Intelligent Robots and Systems (IROS), San Francisco, CA, Sept. 25–30, pp. 973–979.
- [6] Deshpande, A. D., Xu, Z., Weghe, M. J. V., Brown, B. H., Ko, J., Chang, L. Y., Wilkinson, D. D., Bidic, S. M., and Matsuoka, Y., 2013, "Mechanisms of the Anatomically Correct Testbed Hand," *IEEE/ASME Trans. Mechatron.*, **18**(1), pp. 238–250.
- [7] Palli, G., Melchiorri, C., Vassura, G., Scarcia, U., Moriello, L., Berselli, G., Cavallo, A., Maria, G. D., Natale, C., Pirozzi, S., May, C., Ficuciello, F., and Siciliano, B., 2014, "The DEXMART Hand: Mechatronic Design and Experimental Evaluation of Synergy-Based Control for Human-Like Grasping," *Int. J. Robot. Res.*, **33**(5), pp. 799–824.
- [8] Brown, C. Y., and Asada, H. H., 2007, "Inter-Finger Coordination and Postural Synergies in Robot Hands via Mechanical Implementation of Principal Components Analysis," Proceedings of 2007 IEEE/RSJ International

- Conference on Intelligent Robots and Systems, San Diego, CA, Oct. 29–Nov. 2, pp. 2877–2882.
- [9] Xu, K., Liu, H., Du, Y., and Zhu, X., 2014, “Design of an Underactuated Anthropomorphic Hand With Mechanically Implemented Postural Synergies,” *Adv. Robot.*, **28**(21), pp. 1459–1474.
- [10] Xiong, C.-H., Chen, W.-R., Sun, B.-Y., Liu, M.-J., Yue, S.-G., and Chen, W.-B., 2016, “Design and Implementation of an Anthropomorphic Hand for Replicating Human Grasping Functions,” *IEEE Trans. Robot.*, **32**(3), pp. 652–671.
- [11] Xu, K., Liu, Z., Zhao, B., Liu, H., and Zhu, X., 2019, “Composed Continuum Mechanism for Compliant Mechanical Postural Synergy: An Anthropomorphic Hand Design Example,” *Mech. Mach. Theory*, **132**, pp. 108–122.
- [12] Krut, S., Bégoc, V., Dombre, E., and Pierrot, F., 2010, “Extension of the Form-Closure Property to Underactuated Hands,” *IEEE Trans. Robot.*, **26**(5), pp. 853–866.
- [13] Dechev, N., Cleghorn, W., and Naumann, S., 2001, “Multiple Finger, Passive Adaptive Grasp Prosthetic Hand,” *Mech. Mach. Theory*, **36**(10), pp. 1157–1173.
- [14] Lenzi, T., Lipsey, J., and Sensinger, J. W., 2016, “The RIC Arm—A Small Anthropomorphic Transhumeral Prosthesis,” *IEEE/ASME Trans. Mechatron.*, **21**(6), pp. 1–1.
- [15] Pons, J. L., Rocon, E., Ceres, R., Reynaerts, D., Saro, B., Levin, S., and Moorlegem, W. V., 2004, “The MANUS-HAND Dextrous Robotics Upper Limb Prosthesis: Mechanical and Manipulation Aspects,” *Auton. Robots*, **16**(2), pp. 143–163.
- [16] Controzzi, M., Clemente, F., Barone, D., Ghionzoli, A., and Cipriani, C., 2017, “The SSSA-MyHand: A Dexterous Lightweight Myoelectric Hand Prosthesis,” *IEEE Trans. Neural Syst. Rehab. Eng.*, **25**(5), pp. 459–468.
- [17] Baril, M., Laliberté, T., Gosselin, C., and Routhier, F., 2013, “On the Design of a Mechanically Programmable Underactuated Anthropomorphic Prosthetic Gripper,” *ASME J. Mech. Des.*, **135**(12), p. 121008.
- [18] Gosselin, C., Pelletier, F., and Laliberté, T., 2008, “An Anthropomorphic Underactuated Robotic Hand With 15 Dofs and a Single Actuator,” Proceedings of 2008 IEEE International Conference on Robotics and Automation (ICRA), Pasadena, CA, May 19–23, pp. 749–754.
- [19] Belter, J. T., and Dollar, A. M., 2013, “Novel Differential Mechanism Enabling Two DOF From a Single Actuator: Application to a Prosthetic Hand,” Proceedings of 2013 IEEE International Conference on Rehabilitation Robotics (ICORR), Seattle, WA, June 24–26, pp. 1–6.
- [20] Catalano, M. G., Grioli, G., Farnioli, E., Serio, A., Piazza, C., and Bicchi, A., 2014, “Adaptive Synergies for the Design and Control of the Pisa/IIT SoftHand,” *Int. J. Robot. Res.*, **33**(5), pp. 768–782.
- [21] Piazza, C., Catalano, M. G., Godfrey, S. B., Rossi, M., Grioli, G., Bianchi, M., Zhao, K., and Bicchi, A., 2017, “The SoftHand Pro-H: A Hybrid Body-Controlled, Electrically Powered Hand Prosthesis for Daily Living and Working,” *IEEE Robot. Autom. Mag.*, **24**(4), pp. 87–101.
- [22] Biddiss, E., Beaton, D., and Chau, T., 2007, “Consumer Design Priorities for Upper Limb Prosthetics,” *Disabil. Rehabil.: Assist. Technol.*, **2**(6), pp. 346–357.
- [23] Cipriani, C., Controzzi, M., and Carrozza, M. C., 2010, “Objectives, Criteria and Methods for the Design of the SmartHand Transradial Prosthesis,” *Robotica*, **28**(6), pp. 919–927.
- [24] Vinet, R., Lozac’h, Y., Beaudry, N., and Drouin, G., 1995, “Design Methodology for a Multifunctional Hand Prosthesis,” *J. Rehabil. Res. Dev.*, **32**(4), p. 316.
- [25] Østlie, K., Lesjø, I. M., Franklin, R. J., Garfelt, B., Skjeldal, O. H., and Magnus, P., 2012, “Prosthesis Rejection in Acquired Major Upper-Limb Amputees: A Population-Based Survey,” *Disabil. Rehabil.: Assist. Technol.*, **7**(4), pp. 294–303.
- [26] Birglen, L., Gosselin, C., and Laliberté, T., 2008, *Underactuated Robotic Hands*, Springer, New York.
- [27] Lovchik, C. S., and Diftler, M. A., 1999, “The Robonaut Hand: A Dexterous Robot Hand for Space,” Proceedings of 1999 IEEE International Conference on Robotics and Automation (ICRA), Detroit, MI, May 10–15, pp. 907–912.
- [28] Kawasaki, H., Komatsu, T., and Uchiyama, K., 2002, “Dexterous Anthropomorphic Robot Hand With Distributed Tactile Sensor: Giftu Hand II,” *IEEE/ASME Trans. Mechatron.*, **7**(3), pp. 296–303.
- [29] Liu, H., Meusel, P., Seitz, N., Willberg, B., Hirzinger, G., Jin, M. H., Liu, Y. W., Wei, R., and Xie, Z. W., 2007, “The Modular Multisensory DLR-HIT-Hand,” *Mech. Mach. Theory*, **42**(5), pp. 612–625.
- [30] Birglen, L., and Gosselin, C. M., 2006, “Force Analysis of Connected Differential Mechanisms: Application to Grasping,” *Int. J. Robot. Res.*, **25**(10), pp. 1033–1046.
- [31] Xu, K., and Liu, H., 2016, “Continuum Differential Mechanisms and Their Applications in Gripper Designs,” *IEEE Trans. Robot.*, **32**(3), pp. 754–762.
- [32] Schulz, G. R., 1994, *End Effector With Load-Sensitive Digit Actuation Mechanisms*, USPTO, ed., Odetics, Inc., Anaheim, CA, p. 21.
- [33] Takaki, T., and Omata, T., 2006, “100g-100N Finger Joint With Load-Sensitive Continuously Variable Transmission,” Proceedings of 2006 IEEE International Conference on Robotics and Automation, Orlando, FL, May 15–19, pp. 976–981.
- [34] Takaki, T., and Omata, T., 2011, “High-performance Anthropomorphic Robot Hand With Grasping-Force-Magnification Mechanism,” *IEEE/ASME Trans. Mechatron.*, **16**(3), pp. 583–591.
- [35] O’Brien, K. W., Xu, P. A., Levine, D. J., Aubin, C. A., Yang, H.-J., Xiao, M. F., Wiesner, L. W., and Shepherd, R. F., 2018, “Elastomeric Passive Transmission for Autonomous Force-Velocity Adaptation Applied to 3D-Printed Prosthetics,” *Sci. Robot.*, **3**(23), p. eaau5543.
- [36] Plooi, M., Mathijssen, G., Cherelle, P., Lefeber, D., and Vanderborght, B., 2015, “Lock Your Robot: A Review of Locking Devices in Robotics,” *IEEE Robot. Autom. Mag.*, **22**(1), pp. 106–117.
- [37] Controzzi, M., Cipriani, C., and Carrozza, M. C., 2010, “Miniaturized Non-Back-Drivable Mechanism for Robotic Applications,” *Mech. Mach. Theory*, **45**(10), pp. 1395–1406.
- [38] Calli, B., Walsman, A., Singh, A., Srinivasa, S., Abbeel, P., and Dollar, A. M., 2015, “Benchmarking in Manipulation Research: Using the Yale-CMU-Berkeley Object and Model Set,” *IEEE Robot. Autom. Mag.*, **22**(3), pp. 36–52.
- [39] Hill, W., Kyberd, P., Hermansson, L. N., Hubbard, S., Stavdahl, Ø, and Swanson, S., 2009, “Upper Limb Prosthetic Outcome Measures (ULPOM): A Working Group and Their Findings,” *J. Prosthet. Orthot.*, **21**(21), pp. P69–P82.
- [40] Mathiowetz, V., Volland, G., Kashman, N., and Weber, K., 1985, “Adult Norms for the Box and Block Test of Manual Dexterity,” *Am. J. Occup. Ther.*, **39**(6), pp. 386–391.
- [41] Miller, L. A., Stubblefield, K. A., Lipschutz, R. D., Lock, B. A., and Kuiken, T. A., 2008, “Improved Myoelectric Prosthesis Control Using Targeted Reinnervation Surgery: A Case Series,” *IEEE Trans. Neural Syst. Rehabilitation Eng.*, **16**(1), pp. 46–50.